Int. J. Multiphase Flow Vol. 19, No. 6, pp. 1029–1043, 1993
Printed in Great Britain.

0301-9322/93 $6.00 + 0.00

A THREE-LAYER MODEL FOR SOLID–LIQUID FLOW IN HORIZONTAL PIPES

P. DORON and D. BARNEA
Department of Fluid Mechanics and Heat Transfer, Faculty of Engineering, Tel-Aviv University, Ramat-Aviv 69978, Israel

(Received 15 December 1992; in revised form 15 July 1993)

Abstract—A three-layer model for solid–liquid flow in horizontal pipes is proposed. This model overcomes the limitations of the two-layer model. The model predictions exhibit satisfactory agreement with the experimental data and existing correlations.

Key Words: solid–liquid flow, hydraulic transport, slurry flow

INTRODUCTION

The flow of solid–liquid mixtures in horizontal pipes has attracted considerable attention in recent years. It is a very complex flow, due to the presence of the two phases, and is thus quite different from single-phase flow. Since the solid particles tend to settle at the bottom of the pipe various flow patterns may be observed, depending on the mixture flow rate.

Many investigators have tried to develop methods for predicting the characteristics of solid–liquid flow. Two main approaches have been employed: the first is to correlate empirical data, possibly using some semitheoretical reasonings (e.g. Newitt *et al.* 1955; Zandi & Govatos 1967; Turian & Yuan 1977; and many others); the second is to develop theoretical approaches based on phenomenological modeling, such as the two-layer model of Wilson (1976, 1988), Wilson & Pugh (1988) and Televantos *et al.* (1979) or other analyses such as those of Roco & Shook (1985), Hsu *et al.* (1989) and many others. Usually the theoretical models are quite difficult to implement for practical use, while the empirical correlations have a limited range of applicability.

A two-layer model for the prediction of flow patterns and pressure drop was presented by Doron *et al.* (1987). This model is very simple to apply to any set of operational conditions. Its results are quite satisfactory, in spite of the underlying simplifying assumptions.

The main limitation of the Doron *et al.* (1987) two-layer model is its inability to predict accurately enough the existence of a stationary bed at low flow rates. Indeed, there are cases when a stationary bed is observed, yet the model results indicate flow with a moving bed. This also leads to reduced reliability of the pressure drop results for low flow rates (where a stationary bed can be expected). An attempt to solve this shortcoming is presented in this paper, by introducing a three-layer model.

MODEL DESCRIPTION

Suppose a two-phase solid–liquid mixture flows in a horizontal pipe. If the slurry flow rate is high enough, all the solid particles will be suspended. If the flow rate is reduced, the solid particles whose density is higher than that of the carrier fluid, tend to settle and agglomerate at the bottom of the pipe, forming a moving deposit, above which flows a heterogeneous mixture. This behaviour led to the two-layer model of Doron *et al.* (1987). Decreasing the flow rate further causes the moving bed height to increase while its mean velocity decreases. According to the two-layer model, the bed becomes stationary when the sum of the driving forces acting on the bed is lower than the sum of the forces opposing the bed motion. Although the two-layer model performs quite well for flow with a moving bed, it fails in many cases to predict the existence of a stationary bed (which is indeed observed experimentally). It should be noted, that for low mixture flow rates the mean velocities attributed to the moving bed are very low so that the motion may not be observed in reality.

Observations in our laboratory of the flow of solid–liquid mixtures at low flow rates indicate that while the upper strata of the bed may be moving, the lower strata may be stationary. Thus, it is reasonable that at low bed velocities the particles at the bottom get "stuck" and cannot be "dragged" by the bed. This leads to the description of the flow by means of a three-layer model (figure 1), where the bed is actually composed of two layers. The height of the stationary layer is such that the velocity of the moving layer above it is at the particular minimal value which is required for the motion of the particles (i.e. the minimal velocity which causes "stuck" particles to renew their motion). The upper portion of the pipe is occupied by a heterogeneous mixture.

Minimal Bed Velocity

To obtain the minimal velocity of the moving bed, which is a central feature of the three-layer model, as it determines the existence of the three layers, consider the solid particles in the lowermost stratum of the moving layer. Figure 1 presents schematically such a particle, which rests in the "trough" between adjacent particles of the upper part of the stationary bed. The particle is assumed to be at the verge of rolling. In this situation the driving torque (which arises from the drag exerted by the moving bed layer on the particle) and the opposing torque (which arises from the weight of the particle and the moving bed particles) acting on it, must balance. As the magnitudes of these torques depend on the velocity of the moving bed, it can be extracted from the torque balance.

The driving force, F_D, results from the drag exerted by the surrounding medium (i.e. the moving bed layer):

$$F_D = \tfrac{1}{2}\rho_L U_{bc}^2 C_D A_p, \qquad [1]$$

where ρ_L is the density of the carrier liquid, U_{bc} is the critical bed velocity, C_D is the drag coefficient for the particle (based on the particle diameter, d_p, and U_{bc}). A_p is the area upon which the drag force acts, i.e. the projection on a plane normal to the flow direction of the upper part of the particle, which protrudes from the neighboring particles (see figure 1). Hence:

$$A_p = \tfrac{1}{4}\pi d_p^2 - \tfrac{1}{8}d_p^2\left(\frac{\pi}{3} - \sin\frac{\pi}{3}\right) = 0.763 d_p^2. \qquad [2]$$

The torque balance is performed for the point (or axis) of contact of the particle and its neighbors in the downstream direction (denoted by "O" in figure 1). Hence the perpendicular distance to the line of action of the deriving force is

$$L_D = \frac{d_p}{2}\left(\sin\frac{\pi}{3} + 0.0137\right). \qquad [3]$$

The opposing torque is due to the submerged weight of the particle and the solid partices in the bed layer pressing on it. The average number of solid particles whose weight is to be considered is

$$N = C_{mb}\frac{y_{mb} - d_p}{d_p} + 1, \qquad [4]$$

where y_{mb} is the height of the moving bed layer (see figure 2) and C_{mb} is the moving bed

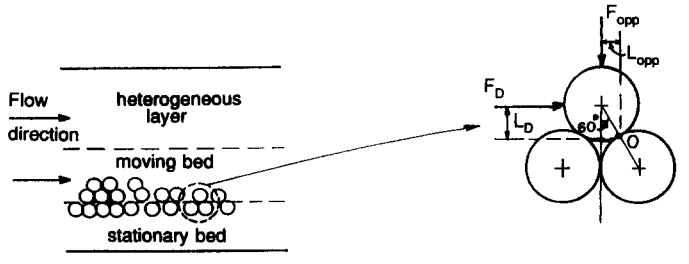

Figure 1. Forces on a particle at the upper stratum of the stationary bed.

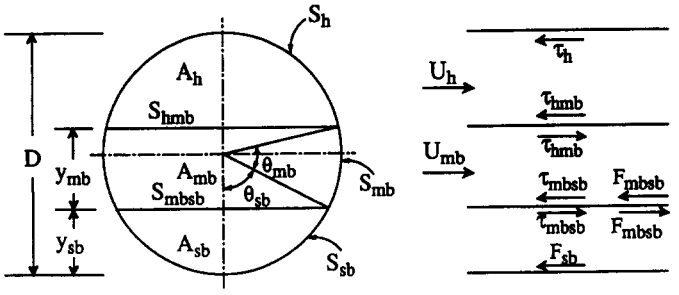

Figure 2. Schematic presentation of the three-layer model; geometry, velocities and shear stresses.

concentration (assumed to be $C_{mb} = 0.52$, for cubic packing). The submerged weight of a particle is

$$W_p = \tfrac{1}{6}\pi(\rho_S - \rho_L)g d_p^3, \qquad [5]$$

where g is the gravitational acceleration and the total opposing force is

$$F_{opp} = W_p\left[C_{mb}\frac{y_{mb}}{d_p} + (1 - C_{mb})\right]. \qquad [6]$$

The perpendicular distance from the line of action of the opposing force to the center of rotation, "O", is

$$L_{opp} = \frac{d_p}{2}\sin\frac{\pi}{6}. \qquad [7]$$

Equating the driving torque ($F_D L_D$) and the opposing torque ($F_{opp} L_{opp}$) yields

$$U_{bc} = \sqrt{\frac{0.779(\rho_s - \rho_L)g d_p\left[C_{mb}\frac{y_{mb}}{d_p} + (1 - C_{mb})\right]}{\rho_L C_D}}; \qquad [8]$$

U_{bc} is the velocity of the moving bed, for which the particles at its bottom are at the verge of rolling. Thus, it is the minimal possible value for the mean velocity of the moving bed. Now suppose that the operational conditions are such that a moving bed with mean velocity U_b is predicted. As the slurry flow rate is reduced, U_b decreases. If it becomes smaller than U_{bc}, a bottom stationary layer is formed, so that the mean velocity of the remaining moving bed layer, U_{mb}, is equal to U_{bc}. A further reduction of the slurry flow rate will induce a build-up of the stationary layer, and a decrease of the moving bed height, y_{mb}. Note that U_{bc} decreases moderately as the slurry flow rate is reduced, since its magnitude is determined by y_{mb} [8].

The Three-layer Model

The whole flow is described by a three-layer model. The analysis is an extension of the analysis of Doron *et al.* (1987) for the two-layer model. Suppose that a solid–liquid mixture flows in a horizontal pipe at a flow rate such that there exist three layers in the pipe: a stationary bed at the bottom; a moving bed above it; and a heterogeneous mixture at the top (figure 2). Obviously, this is an idealization of the physical phenomenon, which assigns mean values to the thicknesses and velocities of the layers.

Continuity

Two continuity equations are written for the two phases:

for the solid particles,

$$U_h C_h A_h + U_{mb} C_{mb} A_{mb} = U_s C_s A; \qquad [9]$$

and

for the liquid phase,

$$U_h(1 - C_h)A_h + U_{mb}(1 - C_{mb})A_{mb} = U_s(1 - C_s)A. \qquad [10]$$

In the above equations U is the axial velocity, C is the volumetric concentration of the solid particles and A is the pipe cross-sectional area; the subscripts h and mb denote the heterogeneous upper layer and the moving bed layer, respectively; U_s is the slurry superficial (mean) velocity, C_s is the slurry input concentration and A_h and A_{mb} are the cross-sectional areas occupied by the dispersed layer and the moving bed, respectively. Note, that based on the results of Doron & Barnea (1992), a no-slip assumption for the bed layers is employed in this formulation (i.e. the mean velocities of the solids and the liquid in each layer are equal). The mean velocity of the lowest layer is zero by definition.

Momentum

Force balances are written for the three layers.

For the upper dispersed layer the heterogeneous mixture is considered as a pseudoliquid with effective properties. Hence:

$$A_h \frac{dP}{dx} = -\tau_h S_h - \tau_{hmb} S_{hmb}; \qquad [11]$$

where dP/dx is the pressure drop, and τ_h and τ_{hmb} are the upper layer shear stress and the interfacial shear stress acting on the perimeters S_h and S_{hmb}, respectively (figure 2).

The shear stress at the pipe circumference is

$$\tau_h = \tfrac{1}{2}\rho_h |U_h| U_h f_h \qquad [12]$$

and the shear stress at the interface between the upper layer and the moving bed is

$$\tau_{hmb} = \tfrac{1}{2}\rho_h |U_h - U_{mb}|(U_h - U_{mb}) f_{hmb}; \qquad [13]$$

ρ_h is the effective density of the upper layer, evaluated as

$$\rho_h = \rho_S C_h + \rho_L (1 - C_h), \qquad [14]$$

where ρ_S and ρ_L are the densities of the solid particles and the liquid, respectively.

The friction coefficient at the pipe wall is found from

$$f_h = \alpha_h \, \mathrm{Re}_h^{-\beta_h}, \qquad [15]$$

where $\alpha_h = 0.046$, $\beta_h = 0.02$ for turbulent flow and $\alpha_h = 16$, $\beta_h = 1$ for laminar flow. The Reynolds number $\mathrm{Re}_h = \rho_h U_h D_h / \mu_L$ is based on the hydraulic diameter $D_h = 4A_h/(S_h + S_{hmb})$.

The friction coefficient at the interface is found from the Colebrook formula, which applies to rough-wall pipes (Streeter &Wylie 1975). It is multiplied by 2, to account for entrainment and deposition of particles, as suggested by Televantos *et al.* (1979). Hence:

$$\frac{1}{\sqrt{2f_{hmb}}} = -0.86 \ln\left(\frac{\frac{d_p}{D_h}}{3.7} + \frac{2.51}{\mathrm{Re}_h \sqrt{2f_{hmb}}}\right), \qquad [16]$$

where the roughness of the interface is assumed of the order of a particle diameter.

For the moving bed layer:

$$A_{mb} \frac{dP}{dx} = -F_{mbsb} - \tau_{mbsb} S_{mbsb} - F_{mb} - \tau_{mb} S_{mb} + \tau_{hmb} S_{hmb}, \qquad [17]$$

where F_{mbsb} is the dry friction force acting at the interface between the moving bed and the stationary bed S_{mbsb}; τ_{mbsb} is the hydrodynamic shear stress acting on that interface; F_{mb} is the dry friction force acting at the surface of contact of the moving bed with the pipe wall, S_{mb}; and τ_{mb} is the hydrodynamic shear acting on that surface.

The shear stress between the moving bed and the pipe wall is expressed by

$$\tau_{mb} = \tfrac{1}{2}\rho_L |U_{mb}| U_{mb} f_{mb} \qquad [18]$$

and the shear at the interface between the moving bed and the stationary bed is

$$\tau_{mbsb} = \tfrac{1}{2}\rho_L |U_{mb}| U_{mb} f_{mbsb}. \qquad [19]$$

The shear stresses are based on ρ_L, following Doron & Barnea (1992).

The friction coefficient at the pipe wall, f_{mb}, is evaluated in a similar way to f_h, [15], i.e.

$$f_{mb} = \alpha_{mb}\,\mathrm{Re}_{mb}^{-\beta_{mb}} \qquad [20]$$

where $\alpha_{mb} = 0.046$, $\beta_{mb} = 0.02$ for turbulent flow and $\alpha_{mb} = 16$, $\beta_{mb} = 1$ for laminar flow. The Reynolds number $\mathrm{Re}_{mb} = \rho_L U_{mb} D_{mb}/\mu_L$ is based on the hydraulic diameter $D_{mb} = 4A_{mb}/(S_{mb} + S_{mbsb})$.

The friction coefficient at the interface between the two bed layers, f_{mbsb}, is evaluated similarly to f_{hmb}, [16]:

$$\frac{1}{\sqrt{2f_{mbsb}}} = -0.86 \ln\left(\frac{d_p}{D_{mb}} + \frac{2.51}{\mathrm{Re}_{mb}\sqrt{2f_{mbsb}}}\right). \qquad [21]$$

F_{mb}, the dry friction force component at the pipe wall contributed by the moving bed solid particles, is composed of the effect of the submerged weight of the particles, F_{Wmb}, and the transmission of stress from the interface, $F_{\phi mb}$:

$$F_{mb} = F_{Wmb} + F_{\phi mb}. \qquad [22]$$

F_{Wmb} is calculated using a pseudohydrostatic pressure distribution which represents the submerged weight of the solid particles, an approximation applicable mainly to coarse particles. Integration of this distribution along the circumference S_{mb}, yields:

$$F_{Wmb} = 2\eta \int_{\theta_{sb}}^{\theta_{mb}+\theta_{sb}} (\rho_S - \rho_L) g C_{mb} \left(\frac{D}{2}\right)^2 \left\{\left[\frac{2(y_{sb} + y_{mb})}{D} - 1\right] - \sin\gamma\right\} d\gamma, \qquad [23]$$

where η is the dry dynamic friction coefficient, g is the gravitational acceleration, D is the pipe diameter, y_{mb} is the height of the moving bed layer, y_{sb} is the height of the stationary bed layer and θ_{mb} and θ_{sb} are the central angles associated with them, respectively (see figure 2).

The shear stress at the interface S_{hmb} is associated with a normal stress, $\tau_N = \tau_{hmb}/\tan(\phi)$, where $\tan(\phi)$ is the tangent of the angle of internal friction, as described first by Bagnold (1954). Following Bagnold's model, which is based on a constant shear stress assumption, the normal stress is transmitted through the packed bed, resulting in a contribution to the frictional resistance, $F_{\phi mb}$:

$$F_{\phi mb} = \eta \frac{\tau_{hmb} S_{mb}}{\tan(\phi)}. \qquad [24]$$

F_{mbsb}, the solid particles contribution to the friction force acting on the interface S_{mbsb}, is found in a similar manner, i.e.

$$F_{mbsb} = F_{Wmbsb} + F_{\phi mbsb}, \qquad [25]$$

where the effect of the submerged weight of the particles is

$$F_{Wmbsb} = \eta(\rho_S - \rho_L) g C_{mb} y_{mb} S_{mbsb} \qquad [26]$$

and the transmission of stress from the interface is represented by

$$F_{\phi mbsb} = \eta \frac{\tau_{hmb} S_{mbsb}}{\tan(\phi)}. \qquad [27]$$

The existence of a stationary bed is determined according to the minimal bed velocity criterion, described in the previous section. In addition, the force balance on the whole stationary bed layer has to be considered. In order for the bed not to slide as a whole, the sum of the driving forces must not exceed the maximal available resistance force [note, that this consideration serves as the criterion for the existence of a stationary bed in the two-layer model of Doron *et al.* (1987)]. This condition should be satisfied whenever a stationary bed is predicted; however, it is not part of the solution process.

The driving forces consist of the pressure gradient and the shear at the interface between the two bed layers. Hence:

$$A_{sb}\frac{dP}{dx} + F_{mbsb} + \tau_{mbsb}S_{mbsb} \leqslant F_{sb}, \quad [28]$$

where A_{sb} is the cross-sectional area of the stationary bed. F_{sb} is the dry friction force acting on the periphery of the stationary bed, S_{sb}. It is evaluated in a similar way to F_{mb}, [22]:

$$F_{sb} = F_{Wsb} + F_{\phi sb}, \quad [29]$$

where the two components are

$$F_{Wsb} = 2\eta_s \int_{-\pi/2}^{\theta_{sb}} (\rho_S - \rho_L)gC_{sb}\left(\frac{D}{2}\right)^2\left[\left(\frac{2y_{sb}}{D} - 1\right) - \sin\gamma\right]d\gamma \quad [30]$$

and

$$F_{\phi sb} = \eta_s \frac{\tau_{hmb}S_{sb}}{\tan(\phi)}, \quad [31]$$

where η_s is the dry static friction coefficient and C_{sb} is the concentration of the stationary bed.

Diffusion

The dispersion of the solid particles in the upper heterogeneous layer is assumed to be governed by the well-known diffusion equation

$$\epsilon\frac{d^2C}{dy^2} + w\frac{dC}{dy} = 0, \quad [32]$$

where y is the vertical coordinate, perpendicular to the pipe axis, ϵ is the diffusion coefficient and w is the terminal settling velocity of the particles. Lateral variations of the concentration are neglected, and the concentration distribution is assumed one-dimensional. Taking the moving bed concentration, C_{mb}, as the boundary condition, the concentration profile in the upper layer is obtained:

$$C(y) = C_{mb}\exp\left(-\frac{w[y - (y_{mb} + y_{sb})]}{\epsilon}\right); \quad [33]$$

w and ϵ are evaluated in the same way as in Doron *et al.* (1987). Upon integration over the cross section of the upper layer, the equation for the mean concentration in that layer, C_h, is obtained:

$$\frac{C_h}{C_{mb}} = \frac{2\left(\frac{D}{2}\right)^2}{A_h}\int_{\theta_{mb}+\theta_{sb}}^{\pi/2}\exp\left\{-\frac{wD}{2\epsilon}[\sin\gamma - \sin(\theta_{mb} + \theta_{sb})]\right\}\cos^2\gamma\, d\gamma. \quad [34]$$

All the geometrical properties which appear in the above equations can be expressed in terms of y_{mb} and y_{sb} for a given pipe diameter, D:

$$A_h = \left(\frac{D}{2}\right)^2\left\{\cos^{-1}\left[\frac{2(y_{mb}+y_{sb})}{D} - 1\right] - \left[\frac{2(y_{mb}+y_{sb})}{D} - 1\right]\sqrt{1 - \left[\frac{2(y_{mb}+y_{sb})}{D} - 1\right]^2}\right\}, \quad [35]$$

$$A_{sb} = \left(\frac{D}{2}\right)^2\left[\pi - \cos^{-1}\left(\frac{2y_{sb}}{D} - 1\right) + \left(\frac{2y_{sb}}{D} - 1\right)\sqrt{1 - \left(\frac{2y_{sb}}{D} - 1\right)^2}\right], \quad [36]$$

$$A_{mb} = \tfrac{1}{4}\pi D^2 - (A_h + A_{sb}), \quad [37]$$

$$S_h = D\cos^{-1}\left[\frac{2(y_{mb}+y_{sb})}{D} - 1\right], \quad [38]$$

$$S_{sb} = D\left[\pi - \cos^{-1}\left(\frac{2y_{sb}}{D} - 1\right)\right], \quad [39]$$

$$S_{mb} = \pi D - (S_h + S_{sb}), \quad [40]$$

$$S_{hmb} = D\sqrt{1 - \left[\frac{2(y_{mb} + y_{sb})}{D} - 1\right]^2}, \quad [41]$$

$$S_{mbsb} = D\sqrt{1 - \left(\frac{2y_{sb}}{D} - 1\right)^2}, \quad [42]$$

$$\theta_{mb} = \cos^{-1}\left(\frac{2y_{sb}}{D} - 1\right) - \cos^{-1}\left[\frac{2(y_{mb} + y_{sb})}{D} - 1\right] \quad [43]$$

and

$$\theta_{sb} = \frac{\pi}{2} - \cos^{-1}\left(\frac{2y_{sb}}{D} - 1\right). \quad [44]$$

The three-layer model is thus described by a set of six equations, [8]–[11], [17] and [34] for the six unknowns U_h, U_{mb} (the mean velocities of the upper layer and of the moving bed, respectively), C_h (the mean concentration of the upper layer), y_{mb}, y_{sb} (the heights of the moving bed and of the stationary bed, respectively) and dP/dx (the pressure gradient).

Mode of solution

We start the solution of the model equations by assuming that a three-layer flow pattern exists. In this case the whole six-equation set is to be solved.

Adding [9] and [10] and rearranging terms yields:

$$U_h = U_s\frac{A}{A_h} + U_{mb}\frac{A_{mb}}{A_h}. \quad [45]$$

Substituting for U_h in [9]:

$$U_s C_h A + U_{mb} C_h A_{mb} + U_{mb} C_{mb} A_{mb} = U_s C_s A \quad [46]$$

and

$$C_h = \frac{U_s C_s A - U_{mb} C_{mb} A_{mb}}{U_s A + U_{mb} A_{mb}}. \quad [47]$$

All the terms on the right-hand side of [45] and [47] are functions of the unknowns y_{mb}, y_{sb} and U_{mb} (as well as the operational conditions). By eliminating the pressure gradient term from [11] and [17] one obtains:

$$\frac{\tau_h S_h + \tau_{hmb} S_{hmb}}{A_h} = \frac{F_{mbsb} + \tau_{mbsb} S_{mbsb} + F_{mb} + \tau_{mb} S_{mb} - \tau_{hmb} S_{hmb}}{A_{mb}}. \quad [48]$$

In [48], too, all the variables can be expressed in terms of y_{mb}, y_{sb} and U_{mb}.

Thus, the set of equations to be solved consists of [8], [34] and [48], with y_{mb}, y_{sb} and U_{mb} as the unknowns (note, that in this case $U_{mb} = U_{bc}$). The three nonlinear equations are solved numerically. In order for the solution to be physically proper the resulting values of the bed heights, y_{sb} and y_{mb}, must be nonnegative and their sum must not exceed the pipe diameter. The value which is obtained for U_{mb} from [8], is always lower than the moving bed velocity obtained by the two-layer model for the same operational conditions. Had it not been the case, the stationary bed height would assume a negative value.

Given any set of operational conditions, for which a stationary bed exists, the flow characteristics can be found by the three-layer model: the heights of the moving bed, y_{mb}, and the stationary bed, y_{sb}, and the mean velocity of the moving bed, U_{mb}, are found by solving the three-equation set, [8], [34] and [48]. The mean velocity of the upper heterogeneous layer, U_h, is found from [45], and its mean concentration, C_h, is found from [47]. The pressure gradient, dP/dx, is then found from [11].

When the stationary bed layer vanishes ($y_{sb} = 0$), there is no solution to [8], [34] and [48] which satisfies the physical constraints and the flow consists of two layers only. In this case [8] becomes redundant, since it only determines the lower limit on U_{mb}, but cannot be used to find its actual

value. The model now reduces to the five-equation set of the two-layer model (Doron *et al.* 1987): [9]–[11] and [34] remain unchanged, whereas [17] reduces to

$$A_{mb}\frac{dP}{dx} = -F_{mb} - \tau_{mb}S_{mb} + \tau_{hmb}S_{hmb}. \quad [49]$$

In addition, $y_{sb} = 0$ is introduced into all the geometrical parameters ([35]–[44]).

After addition and substitution of terms in [9] and [10], one can express the mean velocities in the two layers by means of C_h and y_{mb}:

$$U_h = U_s\frac{A}{A_h}\frac{C_s - C_{mb}}{C_h - C_{mb}} \quad [50]$$

and

$$U_{mb} = U_s\frac{A}{A_{mb}}\frac{C_h - C_s}{C_h - C_{mb}}. \quad [51]$$

Eliminating the pressure term from [11] and [49] yields

$$\frac{\tau_h S_h + \tau_{hmb}S_{hmb}}{A_h} = \frac{F_{mb} + \tau_{mb}S_{mb} - \tau_{hmb}S_{hmb}}{A_{mb}}, \quad [52]$$

where all the terms are functions of C_h, the mean concentration of the upper layer, and y_{mb}, the height of the moving bed. Thus the two-equation set—[34] and [52]—is to be solved numerically for C_h and y_{mb}. The mean velocities of the two layers, U_h and U_{mb}, are then found from [50] and [51], respectively, and the pressure gradient, dP/dx, is calculated using [11].

The transition to fully suspended flow (heterogeneous mixture and homogeneous mixture flow patterns) and the pressure gradient for such flow are treated in the way described in Doron *et al.* (1987).

RESULTS

The first most important feature of the three-layer model is that it does predict the existence of a stationary bed for all sets of operational conditions. Indeed this can be deduced from the postulation of a minimal possible moving bed velocity. Since at the limit of zero flow rate the bed velocity would be zero, there must be a range of slurry flow rates for which the two-layer model would assign a velocity to the moving bed which is lower than the threshold. This is the range of slurry flow rates where the three-layer model comes into effect. The value of the threshold velocity depends on the operational conditions. It may be very small for certain configurations so that in practical systems it would not be actually observed. However, it is always there.

The most important characteristic of the flow is the pressure drop–flow rate relationship. Representative results of the model, showing the effect of the mixture concentration, are presented in figure 3 together with experimental data obtained in our laboratory. The curves represent the predicted dependence of the nondimensional pressure gradient i (expressed in terms of meters of water per meter of pipe length) on the mixture velocity U_s. The theoretical pressure drop curves exhibit quite satisfactory agreement with the data. At the low flow rates where a stationary bed is predicted, the pressure drop is almost independent of the flow rate. This is a bit surprising, since the stationary bed becomes higher as the flow rate is reduced (as will be discussed later). However, the reduction (although slight) of the moving bed mean velocity as well as the drop in the heterogeneous layer mean velocity result in an almost constant pressure gradient. It is important to note, that only few data points could be taken for flow with a stationary bed. At these low flow rates it was very difficult to maintain control over the flow due to the setup of the experimental facility. Nevertheless, the data taken at $C_s = 5.2\%$ and 11% clearly support this trend. Similar behavior was observed by Takaoka *et al.* (1980) for sand slurries (figure 4). In that case, too, the pressure gradient varies only slightly when a stationary bed exists. Additional verification is difficult, since most investigations to date have not considered flow rates below the transition to flow with a stationary bed.

The three-layer model results constitute a significant improvement over the previous two-layer model (Doron *et al.* 1987). For the operational conditions presented in figure 5, for example, the two-layer model predicts only flow with a moving bed. At the low flow rates this causes inaccurate estimates of the pressure gradient (dotted lines in figure 5). The three-layer model, on the contrary, does predict the existence of a stationary bed at the low flow rates, and the resulting pressure gradient is in better agreement with both the experimental data and the Turian & Yuan (1977) correlation, which is based on a very large bank of experimental data (dashed lines in figure 5). Note, that the three-layer model converges to the two-layer model at the higher flow rates, where the two-layer model performs well.

The effect of other operational conditions, such as solids density and pipe diameter, has also been considered (figures 6 and 7). The solid lines represent the three-layer model results, whereas the dashed lines represent Turian & Yuan's (1977) correlation, and the dotted lines represent the two-layer model. In all cases a stationary bed is predicted at the low flow rates, which significantly improves the model performance as compared with the previous two-layer model. Note, that the improved performance is evident also for cases where the previous two-layer model can predict the existence of a stationary bed. The model results were also compared to various sets of experimental data, such as those of Gillies *et al.* (1985) and Thomas (1979), figure 8. In both cases the data refer to flow with no stationary bed, and the data point with the lowest flow rate corresponds to the start-up of the stationary bed. The agreement concerning the pressure gradient as well as the transition to flow with a stationary bed is quite satisfactory.

Figure 9 presents the variation of the bed height (lower part) and the mean moving bed velocity (upper part) with the slurry flow rate for a representative case.

The solid line in the lower part of figure 9 represents the overall height of the bed ($(y_{mb} + y_{sb})/D$) and the dashed line represents the height of the stationary layer (y_{sb}/D). As could be well expected, the bed height decreases as the slurry flow rate is increased, and this trend applies to the stationary layer in particular. However, the moving layer becomes thicker as the slurry flow rate is increased, as long as the three layers exist. For flow rates above the limit deposit velocity (i.e. when there

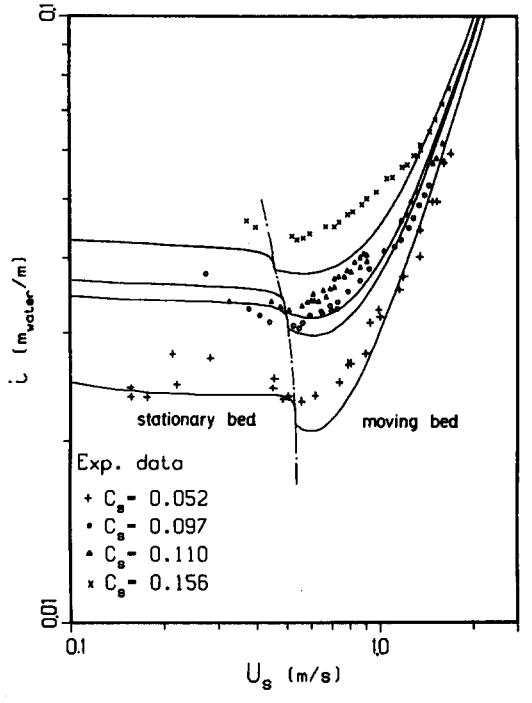

Figure 3. Effect of mixture concentration on the pressure gradient, $\rho_s = 1240$ kg/m^3, $d_p = 3$ mm, $D = 50$ mm: ——, three-layer model; —·—, transition from flow with a stationary bed to flow with a moving bed.

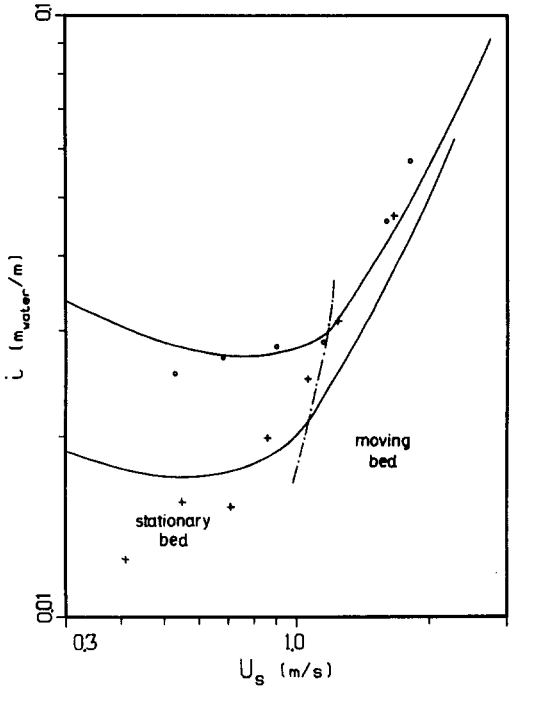

Figure 4. Comparison of experimental data of Takaoka *et al.* (1980), $\rho_s = 2430$ kg/m^3, $d_p = 0.132$ mm, $D = 78$ mm: +, $C_s = 10.3\%$; ○, $C_s = 15.4\%$; ——, three-layer model: —·—, transition from flow with a stationary bed to flow with a moving bed.

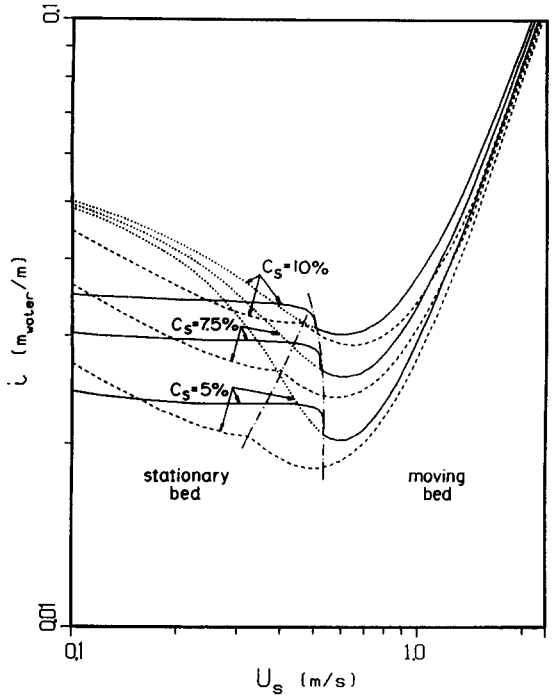

Figure 5. Effect of mixture concentration on the pressure gradient, $\rho_S = 1240$ kg/m^3, $d_p = 3$ mm, $D = 50$ mm: ——, three-layer model; · · · ·, two-layer model (Doron *et al.* 1987); – – –, Turian & Yuan (1977) correlation; —·—, transition from flow with a stationary bed to flow with a moving bed.

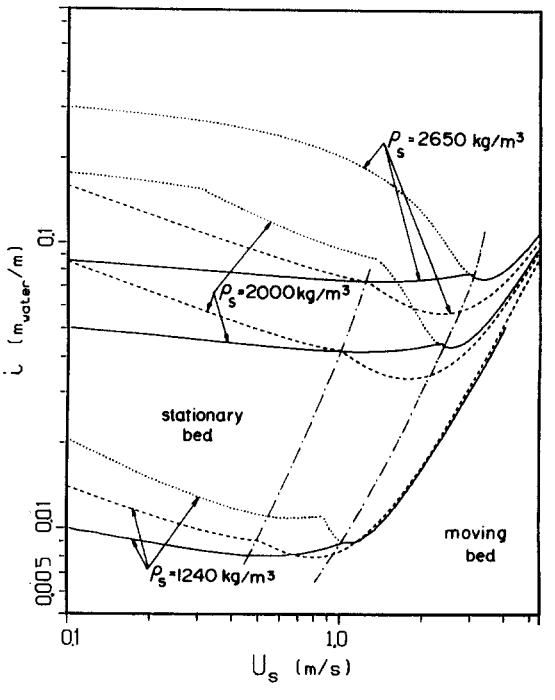

Figure 6. Effect of solids density on the pressure gradient, $C_s = 5\%$, $d_p = 1$ mm, $D = 200$ mm: ——, three-layer model; · · · ·, two-layer model (Doron *et al.* 1987); – – –, Turian & Yuan (1977) correlation; —·—, transition from flow with a stationary bed to flow with a moving bed.

is no stationary bed), the trend is reversed and the moving layer becomes lower for higher velocities. It is interesting to note, that the total height of the two bed layers is quite close to the moving bed height as predicted by the previous two-layer model (dotted line). Nevertheless, as was shown earlier, the pressure gradient is affected very considerably by the type of bed and not just by its overall height. Similar behavior is obtained for other sets of operational conditions.

As noted before, the mean velocity of the moving bed layer, U_{mb}, is a function of the slurry flow rate. However, as can be seen in the upper part of figure 9, its dependence on the mixture velocity is weaker when a stationary bed exists, as compared to flow with a moving bed only as predicted by the two-layer model (dashed line). For this range of operational conditions, the moving bed velocity is determined mainly by the moving bed height (for given solid particles). As described in the previous paragraph, this height increases at a moderate rate until the limit deposit velocity is reached. At higher flow rates, the moving bed mean velocity is determined as part of the solution of the whole set of model equations, and its rate of growth is higher.

The mixture velocity at the limit of existence of a stationary bed, i.e. the limit deposit velocity, U_{LD}, is considered very important for practical purposes. Obviously, it is desired to avoid the formation of stationary deposits, hence it is often regarded as the minimal operating velocity. This velocity can be obtained from the three-layer model when the stationary bed height approaches zero. The value obtained for $y_{sb} = 0$ can be viewed as an upper limit since in practice a bed layer will be considered to vanish when its height is of the order of a particle diameter (and not zero).

The dependence of the limit deposit velocity on the operational conditions can be investigated with the proposed model. Figure 10 presents the effect of mixture concentration on U_{LD}. The model results are in fairly close agreement with the Turian *et al.* (1987) expression and the correlation proposed by Gillies & Shock (1991), which are based on semitheoretical analysis with empirical constants fitting, and they all predict quite a small variation of U_{LD} for these operational conditions (note, that Gillies & Shook's correlation predicts that U_{LD} is independent of C_s for coarse particles). All the predicted results are higher than the experimental data. It is important to note that in the experiments the velocity was reduced until a stationary deposit was observed. It is quite reasonable

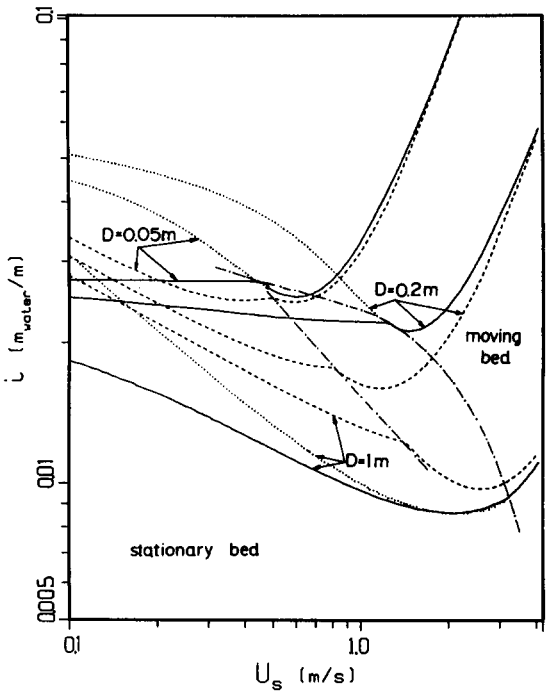

Figure 7. Effect of pipe diameter on the pressure gradient, $\rho_S = 1300\ \text{kg/m}^3$, $C_s = 10\%$, $d_p = 1$ mm: ——, three-layer model; · · ·, two-layer model (Doron *et al.* 1987); – – –, Turian & Yuan (1977) correlation; —·—, transition from flow with a stationary bed to flow with a moving bed.

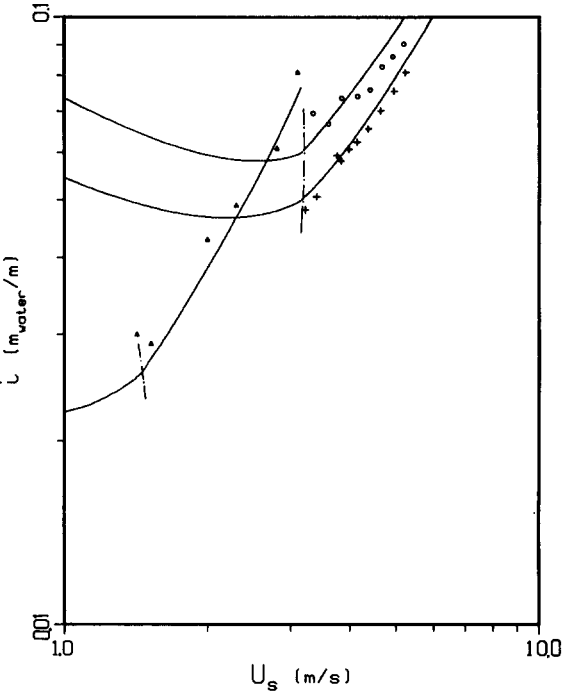

Figure 8. Comparison with experimental data. Gillies *et al.* (1985), $\rho_S = 2650\ \text{kg/m}^3$, $d_p = 0.335$ mm, $D = 260$ mm: +, $C_s = 15\%$; ○, $C_s = 25\%$. △, Thomas (1979), $\rho_s = 2650\ \text{kg/m}^2$, $d_p = 0.150$ mm, $D = 105$ mm, $C_s = 12\%$: ——, three-layer model: —·—, transition from flow with a stationary bed to flow with a moving bed.

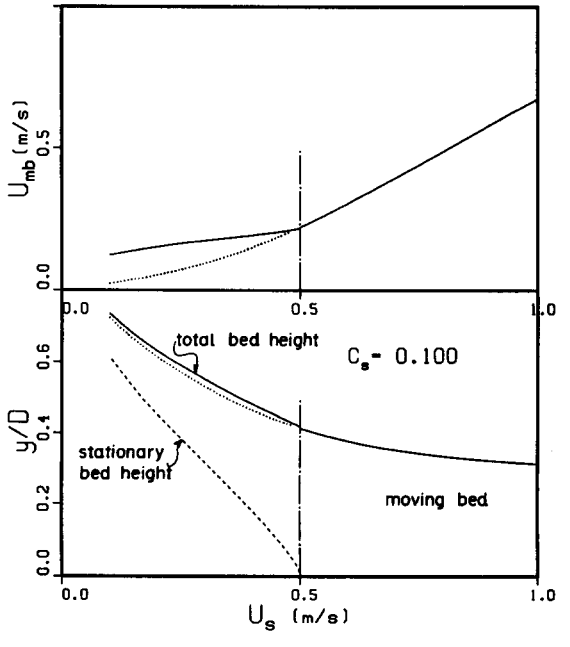

Figure 9. Dependence of bed height and mean moving bed velocity on the mixture velocity, $\rho_S = 1240\ \text{kg/m}^3$, $d_p = 3$ mm, $D = 50$ mm, $C_s = 10\%$: ——, three-layer model; · · ·, two-layer model (Doron *et al.* 1987).

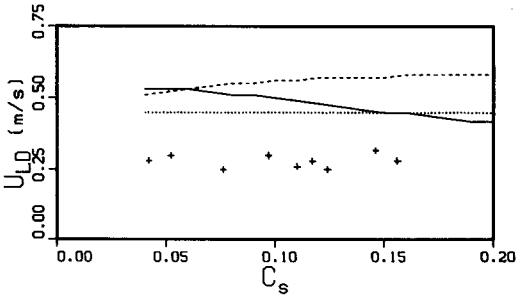

Figure 10. Effect of mixture concentration on the limit deposit velocity, $\rho_s = 1240\ \text{kg/m}^3$, $d_p = 3$ mm, $D = 50$ mm: ——, three-layer model: – – –, Turian *et al.* (1987) correlation; · · ·, Gillies & Shook (1991) correlation; +, experimental data.

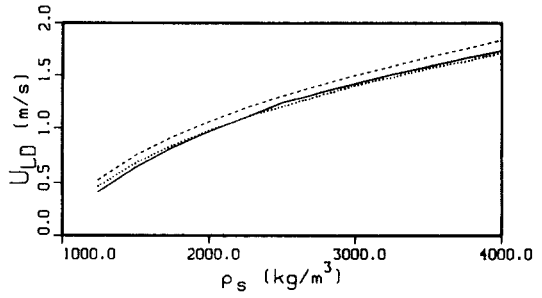

Figure 11. Effect of solids density on the limit deposit velocity, $C_s = 10\%$, $d_p = 1$ mm, $D = 50$ mm: ——, three-layer model; – – –, Turian *et al.* (1987) correlation; · · · ·, Gillies & Shook (1991) correlation.

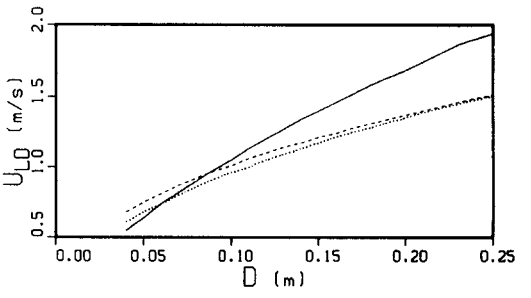

Figure 12. Effect of pipe diameter on the limit deposit velocity, $\rho_s = 1500$ kg/m^3, $d_p = 1$ mm, $C_s = 10\%$: ——, three-layer model; – – –, Turian *et al.* (1987) correlation · · · ·, Gilles & Shook (1991) correlation.

that reversing the procedure would have led to higher observed values. The limit of deposit is closely related to the dry friction, and the value of the static dry friction coefficient is higher than the dynamic one. Thus, it is plausible that a kind of hysteresis effect takes place.

The effect of solids density on the limit deposit velocity is presented in figure 11. Heavier particles require higher driving torques to induce their motion. This can be the result of higher moving bed velocities, which in turn require higher mixture flow rates, i.e. higher U_{LD}.

The pipe diameter also affects the limit deposit velocity. For a larger pipe, the bed would be higher for the same mixture velocity. Thus, a larger mixture velocity would be required to induce the bed motion, i.e. U_{LD} is higher (figure 12). The effect of the pipe diameter can also be deduced from figure 13, which presents the Durand parameter $F_L (F_L = U_{LD}/\sqrt{2gD(s-1)})$ vs the solid particles diameter. According to Durand (1953) and other investigators such as Gillies & Shook (1991), U_{LD} varies as the square root of the pipe diameter. Thus, Durand's data (dashed line) and Gillies & Shook's correlation (dotted line) are represented by single lines in figure 13. The dependence, as predicted by the model (solid lines in figure 13), is quite similar, but not exactly so. Thus, there are different lines for the different values of D. Such an observation was also made by Turian *et al.* (1987), whose correlation is presented by the dashed–dotted lines in figure 13. The model results underpredict Durand's data for the limit deposit velocity (which could result from confusion between the limit deposit velocity and the velocity at the minimal pressure gradient, as explained in the next paragraph). However, they do show the trend of the dependence of U_{LD} on

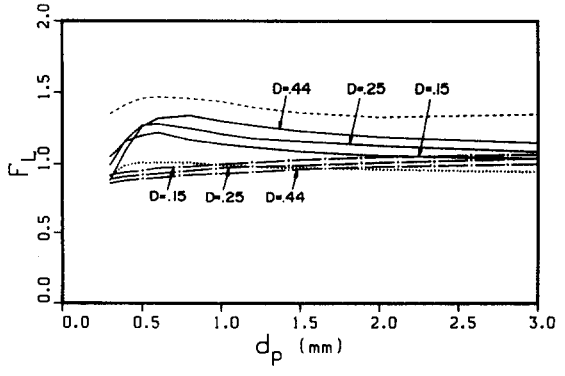

Figure 13. Effect of particle diameter on the Durand parameter F_L, $\rho_s = 2620$ kg/m^3, $C_s = 10\%$: ——, three-layer model; —·—, Turian *et al.* (1987) correlation; · · · ·, Gillies & Shook (1991) correlation; – – – Durand (1953) data.

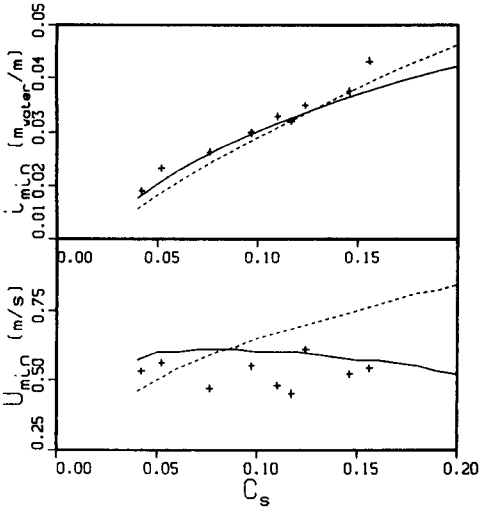

Figure 14. Effect of mixture concentration on the minimal pressure gradient and the corresponding mixture velocity, $\rho_s = 1240$ kg/m^3, $d_p = 3$ mm, $D = 50$ mm: ——, three-layer model; – – –, Turian & Yuan (1977) correlation; +, experimental data.

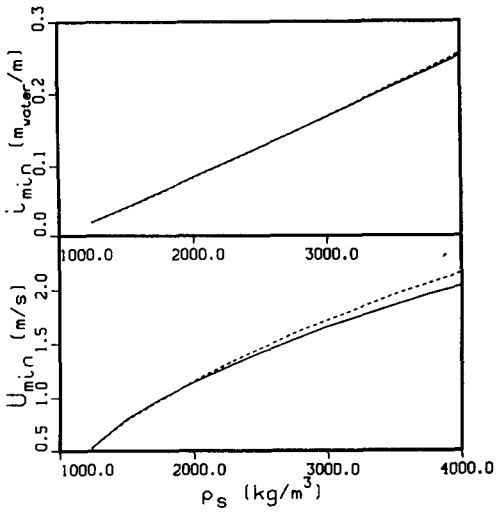

Figure 15. Effect of solids density on the minimal pressure gradient and the corresponding mixture velocity, $C_s = 10\%$, $d_p = 1$ mm, $D = 50$ mm: ——, three-layer model; – – –, Turian & Yuan (1977) correlation.

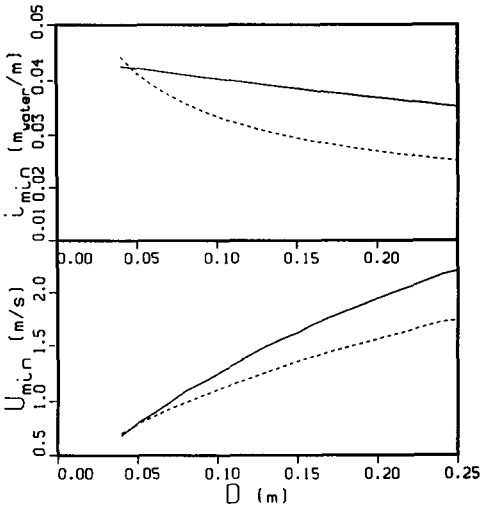

Figure 16. Effect of pipe diameter on the minimal pressure gradient and the corresponding mixture velocity, $\rho_S = 1500$ kg/m^3, $d_p = 1$ mm, $C_s = 10\%$: ——, three-layer model; – – –, Turian & Yuan (1977) correlation.

the particle size. It increases as the particle size is increased, passes through a maximum and approaches an almost constant value for large particles.

Another interesting aspect of the flow is the minimal pressure gradient, i_{min} and the mixture velocity associated with it, i.e. the critial velocity, U_{min}. These can also be found using the proposed model. Many investigators considered the minimum to occur at the limit deposit velocity, an observation which could arise from the very weak dependence of the pressure gradient on the flow rate in the stationary bed flow pattern (as noted before). However, this is not necessarily the case for any set of operational conditions. Actually, in most cases the limit deposit velocity is lower than the critical velocity, so that the minimum occurs in the moving-bed flow pattern range (although there are cases where it is in the stationary-bed flow pattern range). This confusion may be one of the reasons for the overprediction of the limit deposit velocity by the model.

Figure 14 presents the effect of the mixture concentration on the minimal pressure gradient, i_{min}, and the velocity at this minimum, U_{min}. i_{min} increases as the concentration is increased, as predicted by both the model results and the Turian & Yuan (1977) correlation, and verified by the experimental data obtained in our laboratory. This is reasonable, since the higher solids content would require more power for its transportation. U_{min} does not vary much with concentration, as can be observed from the model and from the experimental data. Turian & Yuan's (1977) correlation overpredicts the effect of the concentration on U_{min}.

The effect of the solids density on i_{min} and U_{min} is presented in figure 15. As could be well expected, both i_{min} and U_{min} increase as the solids density is increased, since the settling effects are more significant.

Figure 16 presents the effect of the pipe diameter. Since the limit deposit velocity is higher for larger pipes, so is the critical velocity. The minimal pressure gradient decreases as the pipe diameter is increased. Based on the experience with single-phase flow, where the pressure gradient required for transporting a given flow rate is lower if the pipe is larger, one would expect that the minimal pressure gradient would be reduced for larger diameter pipes. Such a trend can indeed be observed, but the reduction of i_{min} is not very pronounced, because of the increase of U_{min} with pipe size.

SUMMARY

A three-layer model for the prediction of the characteristics of solid–liquid mixtures in horizontal pipes has been presented. This model was developed in order to overcome the limitations of the Doron *et al.* (1987) two-layer model relating to flow with a stationary bed.

The proposed model treats the flow as being constituted of three layers—a stationary layer at the bottom, a moving bed layer above it and a heterogeneous mixture layer at the top. This is based on observations in the laboratory as well as analysis of the flow. The basic assumption underlying the model is the postulation of a minimal velocity which is required to induce the bed motion. If the mean velocity of the moving bed should be reduced below this limiting value, part of it would become stationary, forming the third layer, while the other part would be moving at this minimal velocity. The limiting value for the bed velocity is found by means of a torque balance on a particle at the interface between the stationary and the moving bed layers.

The model results have been compared to experimental data and show satisfactory agreement which amounts to a significant improvement over the performance of the previous two-layer model. This has been shown for a variety of state variables for various sets of operational conditions. Obtaining still better results will be possible when better estimates of the various parameters such as interfacial friction coefficient, diffusion coefficient etc., are available. Moreover, introduction of position-dependent settling velocity and a diffusion coefficient could improve the model performance. However, from our experience the increased accuracy does not justify the far more cumbersome computations required.

REFERENCES

BAGNOLD, R. A. 1954 Experiments on a gravity-free dispersion of large solid spheres in a Newtonian fluid under shear. *Proc. R. Soc. Lond.* **A225,** 49–63.

DORON, P. & BARNEA, D. 1992 Effect of the no-slip assumption on the prediction of solid–liquid flow characteristics. *Int. J. Multiphase Flow* **18,** 617–622.

DORON, P., GRANICA, D. & BARNEA, D. 1987 Slurry flow in a horizontal pipes—experimental and modeling. *Int. J. Multiphase Flow* **13,** 535–547.

DURAND, R. 1953 Basic relationships of the transportation of solids in pipes—experimental research. In *Proc. 5th Minneapolis Int. Hydraulics Convent.*, Minneapolis, MN, pp. 89–103.

GILLIES, R. G. & SHOOK, C. A. 1991 A deposition velocity correlation for water slurries. *Can. J. Chem. Engng* **69,** 1225–1227.

GILLIES, R. G., HUSBAND, W. H. W. & SMALL, M. H. 1985 A study of flow conditions arising in horizontal coarse slurry short distance pipelining practice, phase 1: sand-slurry tests in a 250 mm pipeline. Saskatchewan Research Council, Report No. E833-2-C-85.

HSU, F. L., TURIAN, R. M. & MA, T. W. 1989 Flow of noncolloidal slurries in pipelines. *AIChE Jl* **35,** 429–442.

NEWITT, D. M., RICHARDSON, J. F., ABBOTT, M. & TURTLE, R. B. 1955 Hydraulic conveying of solids in horizontal pipes. *Trans. Instn Chem. Engrs* **33,** 93–113.

ROCO, M. C. & SHOOK, C. A. 1985 Turbulent flow of incompressible mixtures. *J. Fluids Engng* **107,** 224–231.

STREETER, V. L. & WYLIE, E. G. 1975 *Fluid Mechanics.* McGraw-Hill/Kogakusha, Tokyo.

TAKAOKA, T., HISAMITSU, N., ISE, T. & TAKEISHI, Y. 1980 Blockage of slurry pipeline. In *Proc. 7th. Conf. on the Hydraulic Transport of Solids in Pipes*, Sendai, Japan, paper B4, pp. 71–88.

TELEVANTOS, Y., SHOOK, C., CARLETON, A. & STREAT, M. 1979 Flow of slurries of coarse particles at high solids concentrations. *Can. J. Chem. Engng* **57,** 255–262.

THOMAS, A. D. 1979 The role of laminar/turbulent transition in determining the critical deposit velocity and the operating pressure gradient for long distance slurry pipelines. In *Proc. 6th Int. Conf. on the Hydraulic Transport of Solids in Pipes*, Canterbury, U.K., paper A2, pp. 13–26.

TURIAN, R. M. & YUAN, T. F. 1977 Flow of slurries in pipelines. *AIChE Jl* **23,** 232–243.

TURIAN, R. M., HSU, F. L. & MA, T. W. 1987 Estimation of the critical velocity in pipeline flow of slurries. *Powder Technol.* **51,** 35–47.

WILSON, K. C. 1976 A unified physically-based analysis of solid–liquid pipeline flow. In *Proc. 4th Int. Conf. on the Hydraulic Transport of Solids in Pipes*, Banff, Alberta, Canada, paper A1, pp. 1–16.

WILSON, K. C. 1988 Evaluation of interfacial friction for pipeline transport models. In *Proc. 11th*

Int. Conf. on the Hydraulic Transport of Solids in Pipes, Stratford-upon-Avon, U.K., paper B4, pp.107–116.

WILSON, K. C. & PUGH, F. J. 1988 Dispersive-force modelling of turbulent suspension in heterogeneous slurry flow. *Can. J. Chem. Engng* **66**, 721–727.

ZANDI, I. & GOVATOS, G. 1967 Heterogeneous flow of solids in pipelines. *Proc. ASCE Jl Hydraul. Div.* **93**(HY3), 145–159.